

Ionization instabilities and resonant acoustic modes

Xiaogang Wang

Center for Plasma Science and Engineering, Dalian University of Technology, Dalian 116024, People's Republic of China

A. Bhattacharjee, S. K. Gou, and J. Goree

Department of Physics and Astronomy, The University of Iowa, Iowa City, Iowa 52242

(Received 11 April 2001; accepted 5 July 2001)

A linear stability analysis of ion-acoustic and dust-acoustic waves is carried out using a multifluid model in the presence of ionization, ion drag, and collisions of ions and dust with the background neutral gas. It is found that an unstable dust-acoustic mode of nonzero real frequency can be generated via a resonance phenomenon. This resonance develops as the frequency of the dust-ion-acoustic mode is reduced sufficiently in the long-wavelength regime that it couples strongly to the dust-acoustic mode. As the charge on dust particles exceeds a threshold, multiple low-frequency modes with large growth rates are excited suddenly. Predictions of the theory are compared with experimental results [D. Samsonov and J. Goree, *Phys. Rev. E* **59**, 1047 (1999)].

© 2001 American Institute of Physics. [DOI: 10.1063/1.1398283]

I. INTRODUCTION

Recently, there has been considerable experimental and theoretical interest in the ionization instability^{1,2} and its role in exciting dust-ion-acoustic (DIA) and dust-acoustic (DA) modes in dusty plasmas.³⁻¹² Some of the theoretical analyses cited above have been stimulated by recent experimental observations of two new modes.^{3,6} The first mode is called a "filamentary mode" and acts as a precursor to the second, called the "great void mode." Both modes grow after the dust particle size has grown to a sufficient size. The filamentary mode appears first and does so *suddenly* in the form of striations or modulations in the dust density and glow. While the low-frequency density modulations (which peak at about 100 Hz and are broadband) indicate a type of compressional acoustic wave, the glow modulations are suggestive of an ionization wave. After sudden onset, the filamentary mode is seen to evolve to a nonlinear quasisaturated state in less than 10 ms. As the dust particles continue to grow in size, a large void that is entirely free of dust, appears. Unlike the filaments, which appear suddenly, the void grows intermittently, that is, there are transitions back and forth between filaments and void, until the transition ends with the formation of a single large void.

Samsonov and Goree⁶ have suggested that filamentary and void modes may be different dynamical stages of the same instability⁶ and have proposed a mechanism for the instability. This mechanism relies on the imbalance between the electrical and ion drag forces acting on dust particles as the dust particles grow in size. For negatively charged dust particles, the electrical and ion drag forces always oppose each other. This is because, for a given electric field, the electrical force on a negatively charged particle is always antiparallel to the electrical field, but the ion drag force points in the direction of flow of the ions and is parallel to the electric field. These two forces scale differently with dust particle size. Whereas the electrical force scales linearly with

charge and hence the particle radius, the ion drag force scales quadratically with the particle radius. Hence, the electrical force dominates for small particle size (or charge) but the ion drag force dominates for large particle size.

Now, let us suppose that there is a reduction in the density of a spatially uniform dust cloud due to a spontaneous fluctuation. Where the dust density is reduced, there is less depletion of electrons by dust, and, consequently, the electron density and the ionization rate increases. The higher ionization rate produces a positive space charge with respect to the surrounding plasma, and hence an electric field that points outward from the region of reduced dust density. This electric field causes an inward electrical force on negatively charged dust particles that tends to restore the dust density, and an outward force due to the ion drag (in the direction of the ion flow) that tends to expel dust particles from the region of depletion. When the particles are small, the restoring electrical force overcomes the ion drag force, and there is no instability. However, beyond a critical size (and hence, charge) of the dust particles, the ion drag overcomes the electrical force and causes an instability.

The physical picture discussed above has essentially been confirmed by theory.⁷⁻¹² There are, however, a few features of the observations⁶ that need to be addressed, even at the level of linear theory. The first of these is the sudden onset of the instability. While the physical arguments given in Ref. 6 suggest that the instability should appear suddenly when the dust size exceeds a threshold, it is necessary to demonstrate quantitatively that the instability growth rate grows to a very large value for very small increments beyond the threshold. The second observed feature of the instability is that it corresponds to modes with nonzero real frequencies, with a peak around 100 Hz. The third feature is the broadband nature of the spectrum around this 100 Hz peak at a very early stage of the dynamics, suggesting the rapid destabilization of not one, but a broad spectrum of linearly un-

stable, nonzero frequency modes. Our main purpose in this paper is to provide an explanation of these features by extending and building on the foundation of earlier theoretical work,^{7,8} which we briefly review below.

Consistent with the picture proposed by Samsonov and Goree,⁶ D’Angelo⁷ showed that DA modes can be destabilized by the ion drag effect, but the modes he found were ones with zero frequency. Ivlev *et al.*⁸ extended D’Angelo’s analysis by including the effects of ion–neutral collisions and neutral friction. They showed that nonzero frequency ionization instabilities develop due to strong coupling between the DIA and DA modes in a long-wavelength regime, where the ion–neutral collision rate ν_{in} is much larger than the DIA wave frequency (that is, $\nu_{in} \gg kc_{DIA}$, where k is the wave number and c_{DIA} is the phase speed of the DIA). Although the long-wavelength approximation is useful in simplifying the analysis, it is not strictly satisfied in all experiments. We are, therefore, motivated to solve the full dispersion relation numerically. For experimentally relevant parameters, we find that the growth rate does peak for modes with real frequency of the order of 100 Hz. Furthermore, as the threshold for the instability is crossed, the growth rate of the linear instability becomes very large due to a resonance. This resonance occurs as the real frequency of the higher-frequency DIA mode is reduced significantly in the presence of the drag forces, coupling the DIA mode, which is excited by the ionization instability, with the low-frequency DA mode.

It is interesting to note that the resonance is present, even in D’Angelo’s first model, that did not include the ion drag force.⁵ To see this resonance in D’Angelo’s model, one needs to extend the numerical calculation carried out in Ref. 5 to the long-wavelength regime, where the frequency of the DIA mode is so reduced that it couples to the DA mode. D’Angelo did not carry out his numerical calculation in this regime because for the plasma parameters relevant to the experiment discussed by Johnson *et al.*,² the wavelengths were too long to be of relevance for the experiment. As a point of principle, we demonstrate here that it is possible to excite the DA mode, even in the absence of ion drag, through coupling with an unstable DIA mode if the frequency of the DIA mode is sufficiently reduced by some damping mechanism.

The following is the layout of this paper. In Sec. II, we present the multifluid equations underlying our stability analysis. In Sec. III, we derive the dispersion relation for the DIA and DA modes in the appropriate frequency ranges, and demonstrate that the DIA mode frequency is so reduced that it couples with the DA mode, leading to rapid growth of the instability. In Sec. IV, we discuss numerical solutions of the general dispersion relation for the parameters of the experiment and compare the theoretical predictions with experimental data. We conclude the paper with a summary and a discussion of the implications of our results.

II. MULTIFLUID EQUATIONS

The one-dimensional continuity and momentum equations for the dust fluid are given, respectively, by

$$\frac{\partial n_d}{\partial t} + \frac{\partial}{\partial x}(n_d u_d) = 0, \tag{1}$$

and

$$n_d m_d \left(\frac{\partial u_d}{\partial t} + u_d \frac{\partial u_d}{\partial x} \right) - n_d Z e \frac{\partial \phi}{\partial x} + n_d m_d [\nu_{dn} u_d + \nu_{di}(u_d - u_i)] = 0. \tag{2}$$

Here m_d is the mass, $-Ze$ is the (negative) charge, n_d is the density, and u_d is the fluid velocity of dust. The last term on the left of Eq. (2) represents the drag force on the dust particles due to the ions. This drag force is proportional to the dust–ion collision frequency ν_{di} and the relative drift velocity between the dust and ions that move with a fluid velocity u_i . The fourth term represents the frictional drag on dust particles due to collisions at a frequency ν_{dn} with the background neutral gas. The third term represents the self-consistent electric field, given by $-\partial\phi/\partial x$, where ϕ is the electrostatic potential. As in Refs. 7 and 9, we assume that the dust particles are cold. In what follows, we will also not deal with the time variation of the charge Z , considered in Refs. 10–12.

The continuity and momentum equations for ions, of mass m_i , density n_i , and temperature T_i , are given, respectively, by

$$\frac{\partial n_i}{\partial t} + \frac{\partial}{\partial x}(n_i u_i) - Q_i + \nu_L n_i = 0, \tag{3}$$

and

$$n_i m_i \left(\frac{\partial u_i}{\partial t} + u_i \frac{\partial u_i}{\partial x} \right) + n_i e \frac{\partial \phi}{\partial x} + T_i \frac{\partial n_i}{\partial x} + (Q_i - \nu_L n_i) m_i u_i + n_i m_i \nu_{in} u_i + n_i m_i \nu_{id}(u_i - u_d) = 0. \tag{4}$$

In Eqs. (3) and (4), Q_i accounts for ion creation^{5,7} and ν_L is the ion loss rate. In a static, homogeneous and field-free equilibrium, we obtain $Q_{i0} = \nu_L n_{i0}$ from Eq. (3), representing a balance between ion creation and loss. The penultimate term on the left of Eq. (4) represents the frictional drag on the ions due to the neutral gas, with ν_{in} the ion–neutral collision frequency. The last term in Eq. (4) represents the effect of ion–dust collisions on ions that may be ignored in the so-called “collection” regime when the ion Mach number is above unity.¹³ In this regime, considered by D’Angelo,⁷ the ions collide with the dust particles and are lost from the ion fluid. However, the ion Mach number in the experiment^{6,8} is usually below unity and it is in the “orbit” regime where the ions interact with the electric field surrounding the dust, but are not collected by the dust particles. In the “orbit” regime, it is important to retain the momentum transfer to the ion fluid by the dust. From momentum conservation between ions and dust, we obtain

$$n_d m_d \nu_{di}(u_d - u_i) + n_i m_i \nu_{id}(u_i - u_d) = 0, \tag{5}$$

which implies that

$$\nu_{di} = \frac{n_i m_i}{n_d m_d} \nu_{id} \equiv \frac{m_i}{\epsilon m_d} \nu_{id} \ll \nu_{id}. \tag{6}$$

For the electrons of density n_e and temperature T_e , we neglect inertia and use the Boltzmann response,^{4–12}

$$-n_e e \frac{\partial \phi}{\partial x} + T_e \frac{\partial n_e}{\partial x} = 0. \quad (7)$$

Finally, the self-consistent electrostatic potential is determined from the quasineutrality constraint

$$n_e + Zn_d = n_i. \quad (8)$$

III. THE DISPERSION RELATIONS

We now solve the linearized forms of Eqs. (1)–(8), assuming a homogeneous, static, field-free equilibrium that obeys the conditions $Q_{i0} = \nu_L n_{i0}$ and $n_{i0} = n_{e0} + Zn_{d0}$. In general, the ion creation can be written as,^{5,7,9,14} $Q_I = \nu_I n_e$, where ν_I is the ionization frequency. In equilibrium, we have $Q_{I0} = \nu_{I0} n_{e0} = \nu_L n_{i0}$, so the equilibrium ionization rate is given by $\nu_{I0} = \nu_L n_{i0} / n_{e0} = \nu_L / (1 - \epsilon Z)$. The perturbed ion creation term can be written as

$$\begin{aligned} \tilde{Q}_I &= \nu_{I0} \tilde{n}_e + n_{e0} \frac{\partial \nu_{I0}}{\partial n_{e0}} \tilde{n}_e \\ &= \nu_{I0} \left(1 + \frac{n_{e0}}{\nu_{I0}} \frac{\partial \nu_{I0}}{\partial n_{e0}} \right) \tilde{n}_e \\ &= \frac{\nu_L}{(1 - \epsilon Z)} \left(1 + \frac{n_{e0}}{\nu_{I0}} \frac{\partial \nu_{I0}}{\partial n_{e0}} \right) \tilde{n}_e \\ &\equiv \alpha \nu_L \tilde{n}_e = \alpha \nu_L (\tilde{n}_i - Z \tilde{n}_d), \end{aligned} \quad (9)$$

where

$$\alpha \equiv \frac{1}{(1 - \epsilon Z)} \left(1 + \frac{n_{e0}}{\nu_{I0}} \frac{\partial \nu_{I0}}{\partial n_{e0}} \right) > 1.$$

In what follows, we use the continuum ionization model¹⁴ in which $\partial \nu_{I0} / \partial n_{e0} = 0$, and $\alpha = 1 / (1 - \epsilon Z)$.

We carry out a simple one-dimensional analysis assuming that all perturbed quantities can be written in the plane-wave form, $\exp(ikx - i\omega t)$. The linearized ion momentum equation (4) yields

$$-i\omega \tilde{u}_i + ik [c_{IA}^2 (\tilde{n}_i - Z \tilde{n}_d) + v_i^2 \tilde{n}_i] + n_{i0} \nu_{id} (\tilde{u}_i - \tilde{u}_d) = 0, \quad (10)$$

where $c_{IA} \equiv [T_e / m_i (1 - \epsilon Z)]^{1/2}$ is the DIA speed, and $v_i \equiv (T_e / m_i)^{1/2}$ is the ion thermal speed. The linearized ion continuity equation (3) gives

$$-i\omega \tilde{n}_i + ik n_{i0} \tilde{u}_i - (\alpha - 1) \nu_L \tilde{n}_i + \alpha \nu_L Z \tilde{n}_d = 0. \quad (11)$$

Defining $\hat{n}_i \equiv \tilde{n}_i / n_{i0}$, $\hat{n}_d \equiv \tilde{n}_d / n_{d0} = \tilde{n}_d / (\epsilon n_{i0})$, from Eqs. (10) and (11), we obtain

$$\begin{aligned} [\omega(\omega + i\beta_i) - (k^2 c_s^2 - \omega_{iv}^2)] \hat{n}_i + [\epsilon Z (k^2 c_{IA}^2 - \gamma_{iv}^2) \\ + i\omega(\epsilon Z \alpha \nu_L - \nu_{id})] \hat{n}_d = 0, \end{aligned} \quad (12)$$

where

$$\begin{aligned} c_s^2 &= c_{IA}^2 + v_i^2, \\ \beta_i &\equiv \nu_{id} + \nu_{in} - (\alpha - 1) \nu_L, \\ \omega_{iv}^2 &\equiv (\alpha - 1) \nu_L (\nu_{id} + \nu_{in}), \\ \gamma_{iv}^2 &\equiv \alpha \nu_L (\nu_{id} + \nu_{in}) = [\alpha / (\alpha - 1)] \omega_{iv}^2. \end{aligned}$$

We linearize the dust equations (1) and (2) to obtain

$$\begin{aligned} -i\omega \hat{n}_d + ik \tilde{u}_d &= 0, \quad (13) \\ -i\omega \tilde{u}_d + \nu_{dn} \tilde{u}_d + \nu_{di} (\tilde{u}_d - \tilde{u}_i) - ik c_{DA}^2 (\hat{n}_i / \epsilon Z - \hat{n}_d) &= 0. \quad (14) \end{aligned}$$

From Eqs. (13) and (14), we obtain

$$\begin{aligned} [\omega(\omega + i\beta_d) - (k^2 c_{DA}^2 - \omega_{dv}^2)] \hat{n}_d \\ + [(k^2 c_{DA}^2 - \gamma_{dv}^2) / \epsilon Z - i\omega \nu_{di}] \hat{n}_i = 0, \end{aligned} \quad (15)$$

where $c_{DA} \equiv [\epsilon Z^2 T_e / m_d (1 - \epsilon Z)]^{1/2}$ is the DA wave speed, and

$$\begin{aligned} \beta_d &\equiv \nu_{dn} + \nu_{di}, \\ \omega_{dv}^2 &\equiv \epsilon Z \alpha \nu_L \nu_{di}, \\ \gamma_{dv}^2 &\equiv \epsilon Z (\alpha - 1) \nu_L \nu_{di} = (1 - 1/\alpha) \omega_{dv}^2. \end{aligned}$$

From Eqs. (12) and (15), we obtain the dispersion relation

$$\begin{vmatrix} \omega(\omega + i\beta_i) - (k^2 c_s^2 - \omega_{iv}^2) & \epsilon Z (k^2 c_{IA}^2 - \gamma_{iv}^2) + i\omega(\epsilon Z \alpha \nu_L - \nu_{id}) \\ (k^2 c_{DA}^2 - \gamma_{dv}^2) / \epsilon Z - i\omega \nu_{di} & \omega(\omega + i\beta_d) - (k^2 c_{DA}^2 - \omega_{dv}^2) \end{vmatrix} = 0. \quad (16)$$

A. Ion-acoustic waves

In the range of $kc_{DA} \ll kv_i \ll \omega \ll kv_e$, the dispersion relation (16) can be approximated as

$$\begin{vmatrix} \omega(\omega + i\beta_i) - (k^2 c_s^2 - \omega_{iv}^2) & i\omega(\epsilon Z \alpha \nu_L - \nu_{id}) \\ -i\omega \nu_{di} & \omega^2 \end{vmatrix} = 0, \quad (17)$$

or

$$\omega(\omega + i\beta_i) = k^2 c_s^2 - \omega_{i0}^2, \quad (18)$$

where $\omega_{i0}^2 \equiv \nu_L [(\alpha - 1)(\nu_{id} + \nu_{in}) + \alpha \nu_{di}] - \nu_{id} \nu_{di} \approx (\alpha - 1) \nu_L (\nu_{id} + \nu_{in})$. The dispersion relation (18) yields two ion-acoustic branches, given by

$$\omega_{\pm} = \pm \left[k^2 c_s^2 - \left(\omega_{i0}^2 + \frac{\beta_i^2}{4} \right) \right], \quad (19)$$

if $k^2 c_s^2 > (\omega_{i0}^2 + \beta_i^2/4)$. Both branches have the same growth rate, given by

$$\gamma_{\pm} = -\frac{\beta_i}{2} \equiv \left(\frac{\alpha}{2} - 1\right) \nu_L - \frac{\nu_{id} + \nu_{in}}{2}. \quad (20)$$

On the other hand, if $k^2 c_s^2 \leq (\omega_{i0}^2 + \beta_i^2/4)$, both waves become purely growing, with

$$\omega_{\pm} = 0, \quad (21)$$

$$\gamma_{\pm} = -\frac{\beta_i}{2} \pm \left[\left(\omega_{i0}^2 + \frac{\beta_i^2}{4} \right) - k^2 c_s^2 \right]. \quad (22)$$

Equation (18) shows that the frequency of the DIA modes is reduced by the effects of ionization as well as frictional and drag forces. If the DIA mode frequency is so reduced that it becomes comparable to the DA mode frequency, it is reasonable to expect strong coupling and possible destabilization of a low-frequency instability.

B. Low-frequency modes and resonant destabilization

In the range $k c_{DA} \sim \omega \ll k v_i$, the dispersion relation (16) can be approximated as

$$\begin{vmatrix} -(k^2 c_s^2 - \omega_{iv}^2) & \epsilon Z (k^2 c_{IA}^2 - \gamma_{iv}^2) + i \omega (\epsilon Z \alpha \nu_L - \nu_{id}) \\ (k^2 c_{DA}^2 - \gamma_{dv}^2) / \epsilon Z & \omega (\omega + i \beta_d) - (k^2 c_{DA}^2 - \omega_{dv}^2) \end{vmatrix} = 0, \quad (23)$$

or

$$\omega (\omega + i \beta'_d) - (k^2 c_{DA}^2 - \omega_{d0}^2) = 0, \quad (24)$$

where

$$\beta'_d \equiv \beta_d + \frac{(k^2 c_{DA}^2 - \gamma_{dv}^2) (\epsilon Z \alpha \nu_L - \nu_{id})}{\epsilon Z (k^2 c_s^2 - \omega_{iv}^2)},$$

$$\omega_{d0}^2 \equiv \omega_{dv}^2 + \frac{(k^2 c_{IA}^2 - \gamma_{iv}^2) (k^2 c_{DA}^2 - \gamma_{dv}^2)}{k^2 c_s^2 - \omega_{iv}^2}.$$

The two branches of the dispersion relation (24) are

$$\omega_{\pm} = \pm \left[k^2 c_{DA}^2 - \left(\omega_{d0}^2 + \frac{\beta_d'^2}{4} \right) \right]^{1/2}, \quad (25)$$

if $k^2 c_{DA}^2 > (\omega_{d0}^2 + \beta_d'^2/4)$. Both branches exhibit the same growth rate, given by

$$\gamma_{\pm} = -\frac{\beta_d'}{2} = -\frac{\beta_d}{2} - \frac{(k^2 c_{DA}^2 - \gamma_{dv}^2) (\epsilon Z \alpha \nu_L - \nu_{id})}{2 \epsilon Z (k^2 c_s^2 - \omega_{iv}^2)}. \quad (26)$$

From the condition

$$k^2 c_{DA}^2 > \left(\omega_{d0}^2 + \frac{\beta_d'^2}{4} \right) > \omega_{dv}^2 = \epsilon Z \alpha \nu_L \nu_{di} > \epsilon Z (\alpha - 1) \nu_L \nu_{di} = \gamma_{dv}^2,$$

we see that the two branches given by (25) are stable in the short-wavelength regime, $k^2 c_s^2 > \omega_{iv}^2 \gg \omega^2$.

In the parameter range $k^2 c_{DA}^2 \leq (\omega_{d0}^2 + \beta_d'^2/4)$, both branches yield purely growing modes, with

$$\omega_{\pm} = 0, \quad (27)$$

$$\gamma_{\pm} = -\frac{\beta_d'}{2} \pm \left[\left(\omega_{d0}^2 + \frac{\beta_d'^2}{4} \right) - k^2 c_{DA}^2 \right]^{1/2}. \quad (28)$$

Clearly, the ω_+ branch is unstable in the range

$$\omega_{iv}^2 / c_s^2 < k^2 < \omega_{d0}^2 / c_{DA}^2. \quad (29)$$

In the short-wavelength range, $k^2 c_s^2 > \omega_{iv}^2 \gg \omega^2$, the inequality (29) indicates instability if

$$\nu_{di} > \frac{c_{DA}^2 [\nu_L (\nu_{id} + \nu_{in}) + k^2 \nu_i^2]}{\epsilon Z \nu_L (c_{IA}^2 + \alpha \nu_i^2)} \equiv \nu_{di,crit}, \quad (30)$$

which is essentially equivalent to the result obtained in Ref. 7 [except for a difference attributable to the presence of the ion–dust collisional term in the ion momentum equation (4)].

For the nonzero frequency branches described by Eqs. (25) and (26), as $k^2 c_s^2$ approaches ω_{iv}^2 from below, we obtain very rapidly growing DA modes. This rapidly growing instability is due to the resonance $k^2 c_s^2 = \omega_{iv}^2$.

IV. NUMERICAL SOLUTIONS OF THE FULL DISPERSION EQUATION AND A COMPARISON WITH EXPERIMENTS

The discussions in Sec. III are based on asymptotic approximations of the full dispersion relation (16). In particular, the slowing down of the DIA wave is based on the DIA dispersion relation (18), which is derived under the approximation $k c_{DA} \ll k v_i \ll \omega \ll k v_e$. As the DIA wave frequency is so reduced that it approaches the DA frequency $k c_{DA}$, the approximation is not valid anymore, and we need to solve the full general dispersion (16).

In this section, we describe numerical solutions of the dispersion equation (16) for two sets of parameters: one set corresponds to the experiments of Samsonov and Goree,⁶ the other is the same as D’Angelo’s.⁵ In both cases, it is shown that in the long-wavelength regime, the frequency of the DIA branches is indeed reduced and resonant destabilization occurs in the manner predicted in Sec. III.

The density and temperature parameters of the experiment are (3,6) $T_e \approx 3$ eV, $T_i \approx 0.025$ eV–0.1 eV, $n_i \approx 2 \times 10^9$ cm⁻³, $n_d \approx 10^7$ cm⁻³, $Z \approx 75$, $m_i = 40 m_p$, and $m_d / m_i \approx 2 \times 10^7$. The dust particle radius is approximately given by $a_d \approx 0.05$ μm. The temperature and filling pressure of the background gas is approximately 0.025 eV and 400 mTorr, respectively. Using the continuum ionization model¹⁴ mentioned in Sec. III, we obtain $\alpha \equiv (1 - \epsilon Z)^{-1} \approx 2$. From the code SIGLO-2D¹⁵ which simulates a glow discharge without dust, we obtain the ion–neutral collision rate $\nu_{in} \sim 10^6$ s⁻¹, and the ion loss rate $\nu_L \approx 5 \times 10^5$ s⁻¹. Also, making use of the formulas in Refs. 16 and 17 for ν_{dn} and calculating ν_{di} from the treatment given in the Appendix, we obtain $\nu_{dn} \approx 5.6 \times 10^3$ s⁻¹ $\ll \nu_{id} = (\epsilon m_d / m_i) \nu_{di} \approx 3.47 \times 10^5$ s⁻¹, $c_{IA} \approx 2.8 \times 10^5$ cm s⁻¹, $c_{DA} \approx 7 \times 10^2$ cm s⁻¹, and $\nu_i \approx 3.5 \times 10^4$ cm s⁻¹.

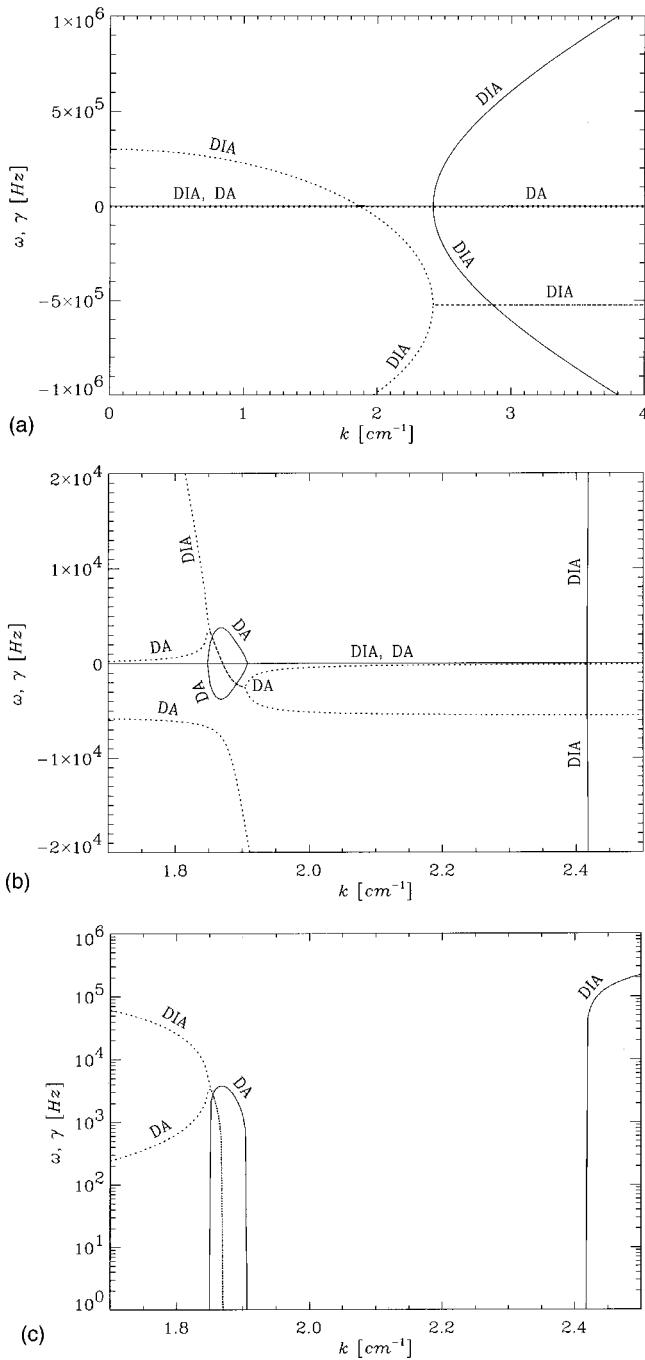


FIG. 1. Frequency ω (solid line) and growth rate γ (dashed line) in Hz of DIA and DA modes as a function of the wave number k (cm^{-1}), using the parameters of the experiment. Note that (b) is a magnified view of part of (a) in the vicinity of the resonance, while (c) is a plot of modes with positive ω and γ in a logarithmic scale.

In Figs. 1(a)–1(c), we show the real (solid line) and imaginary part (the growth rate, dotted line) of the complex frequency (in Hz) as a function of wave number k (in cm^{-1}). Figure 1(a) gives a complete plot of the roots of the dispersion equation, including stable as well as unstable branches. We note that the high-frequency ($\sim 10^5$ – 10^6 Hz) DIA modes are stable in the short-wavelength (large k) regime, with a flat (negative) growth rate of approximately $-2 \times 10^5/\text{s}$. The region of instability occurs near $k \sim 2 \text{ cm}^{-1}$ when the DIA frequency is reduced sufficiently that it can couple with the

DA mode. In order to exhibit clearly the nature of the resonance that gives rise to instability, we show in Fig. 1(b) a magnified version of the resonant region in Fig. 1(a). Figure 1(c) is similar to Fig. 1(b), except that it shows only the modes with a positive real frequency and growth rate in the resonant region on a logarithmic scale. Figure 1(b) shows clearly that as the wave number k decreases from 2.20 cm^{-1} to lower values, a bifurcation occurs in the DA branches at $k \approx 1.90 \text{ cm}^{-1}$ before the resonance at $k_r \approx 1.87 \text{ cm}^{-1}$. If we track the growth-rate curves for the different modes, we find that while one of the DIA modes for $k > k_r$ continues as a DA mode for $k < k_r$, one of the DIA modes for $k < k_r$ continues as a DA mode for $k > k_r$. In other words, there is an exchange of stability properties at the resonance. Near the resonance, the growth rate of the coupled mode increases very sharply, accounting for an important qualitative feature of the experiment. Furthermore, we note that the resonance, which is sharp in wave number, encompasses a broad spectrum of nonzero frequencies.

From Eq. (25), the condition $\omega_{\pm}^2 > 0$ requires that

$$k^2 c_{\text{DA}}^2 \left(\omega_{d0}^2 + \frac{\beta_d'^2}{4} \right) > \omega_{dv}^2 = \epsilon Z \alpha \nu_L \nu_{\text{di}}. \quad (31)$$

These two branches are stable unless $k^2 c_s^2$ tends to ω_{iv}^2 from below, and

$$k^2 c_s^2 \approx k^2 c_{\text{IA}}^2 < \omega_{iv}^2. \quad (32)$$

Combining Eqs. (31) and (32), the condition for the instability can be written as

$$Z > Z_c \equiv \frac{\alpha \nu_{\text{id}}}{\epsilon(\alpha - 1)(\nu_{\text{in}} + \nu_{\text{id}})}. \quad (33)$$

Using the parameters of the experiment,⁶ $\epsilon = n_d/n_i = 5 \times 10^{-3}$, $\nu_{\text{id}} = 3.47 \times 10^5 \text{ s}^{-1}$, and $\nu_{\text{in}} \approx 10^6 \text{ s}^{-1}$, we estimate that the critical dust charge for the onset of the instability is given by $Z_c \approx 100$, which is higher by about 20% than the observations. In order to obtain a more precise estimate of Z_c from the full dispersion equation in Fig. 2, we show the frequency and growth rate of the mode as a function of the dust charge Z for the wave number $k = 2\pi/L \approx 2.3 \text{ cm}^{-1}$, where $L = 2.6 \text{ cm}$ is the half-length of the system. Inspection shows that in this case $Z_c = 110$, which is close to the estimated observed value. Figure 2 also shows that there is a broad range of nonzero real frequencies, including 100 Hz, that are driven unstable with a very large growth rate just after the threshold is crossed, qualitatively in accord with the experiment.

As discussed in Sec. I, the picture described above applies to D'Angelo's basic model,⁵ even without ion drag or the other effects discussed in subsequent analyses.^{7,9–12} Apparently, D'Angelo did not consider this possibility because, for the parameters he chose, it would have taken him outside the range of wavelengths that were relevant for the experiment of Johnson *et al.*² We have carried out a full analysis of the dispersion equation for the parameters used by D'Angelo.⁵ (These parameters are quite different from the ones we have used above.) We do recover the results of Ref. 5 in the short-wavelength (large k) regime, where two un-

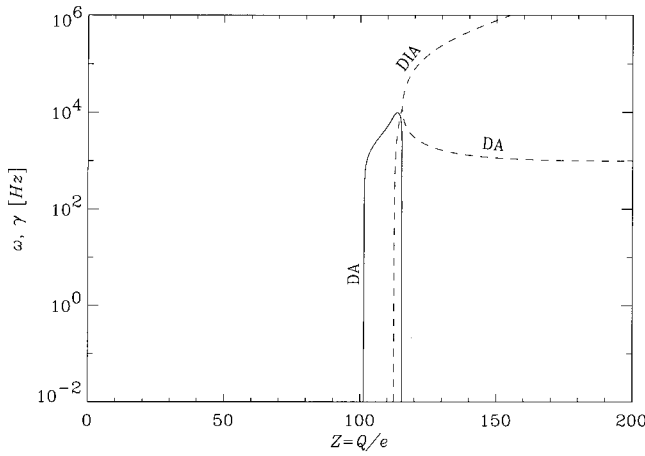


FIG. 2. Logarithmic plot of positive ω (solid line) and growth rate γ (dashed line) in Hz of DIA and DA modes as a function of the dust charge Z for a fixed wave number $k=2.3 \text{ cm}^{-1}$.

stable branches of high-frequency ($\sim 10^5 \text{ Hz}$) DIA modes and two very weakly damped low-frequency ($\sim 10^2 \text{ Hz}$) DA modes are identified. However, as shown in Fig. 3, in the long-wavelength (small k) regime, a resonant destabilization of DA modes occurs as the frequency of the DIA modes is so reduced that it matches the frequency of the DA modes.

V. SUMMARY

Prompted by the experimental observations of Samsonov and Goree,⁶ we have carried out a linear analysis of the stability of DA and DIA modes in a multifluid model in the presence of ionization, ion drag, and collisions of ions and dust with the background neutral gas. We have built on the foundation of other calculations,^{5,7,9-12} and attempted to explain some of the key features of the observations. Our principal result is that in the long-wavelength regime, the frequency of the DIA modes is sufficiently reduced that they couple strongly to the DA modes via a resonance. Under these conditions, when the dust particle charge exceeds a threshold, multiple nonzero frequency modes of very large

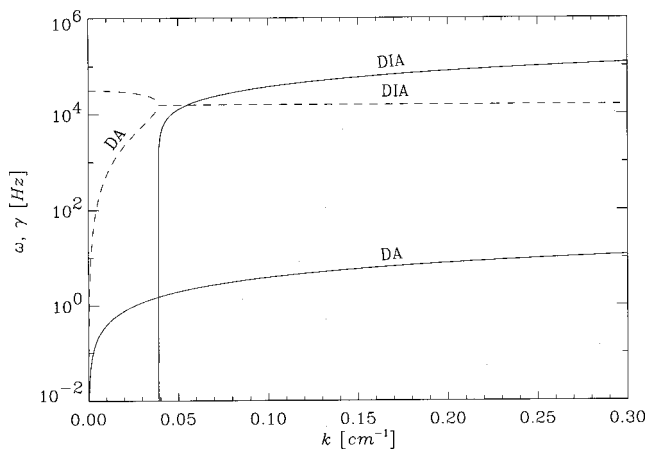


FIG. 3. Logarithmic plot of ω (solid line) and growth rate γ (dashed line) in Hz of DIA and DA modes as a function of the wave number k (cm^{-1}), using the parameters given in Ref. 5.

growth rates are produced, accounting for some of the observed features of the filamentary instability. Although ion drag does play an important role in the experiment discussed by Samsonov and Goree,⁶ it is not essential for the coupling between the DIA and DA modes. Thus, the instability mechanism discussed in this paper may be operative in other contexts where the ion drag force is less important.

Our theory is linear, and cannot account for the nonlinear evolution of the filamentary instabilities. As the linear instability has very high growth rate, nonlinear effects should become important relatively quickly during its evolution. The experimental evidence suggests that the mode saturates to form a void, for which a steady-state model has been given in Ref. 8. An interesting question is whether the present model, in its nonlinear variant, can show a way of connecting the linear dynamics to the saturated void structure discussed in Ref. 8. This will be the subject of a future investigation.

ACKNOWLEDGMENTS

We thank N. D’Angelo, S. Hu, and K. Avinash for useful discussions.

This research is supported by NASA Grants No. NAG5-2375 and No. NAG3-2128, and Department of Energy (DOE) Grant No. DE-FG02-00ER54607.

APPENDIX: CALCULATION OF THE ION DRAG

We calculate the ion drag force using the Rosenbluth potential from Fokker–Planck theory.¹⁸ It can be shown that the force on an ion by dust particles when the ion is streaming with a velocity v_s with respect to the dust is given by

$$F_{id} = - \left(1 + \frac{m_i}{m_d} \right) \frac{4 \pi n_d e^4 Z^2 \Gamma}{m_i v_s^2} \psi(x_{id}), \tag{A1}$$

where $\Gamma \equiv \ln \Lambda$ is the Coulomb logarithm, and v_s is given by^{6,13}

$$v_s \approx \sqrt{\frac{8T_i}{\pi m_i} + v_{ith}^2} \approx 1.51 v_{ith}.$$

Here the Rosenbluth integral $\psi(x_{id})$ is defined as

$$\psi(x_{id}) = \frac{2}{\sqrt{\pi}} \int_0^{x_{id}} t^{1/2} e^{-t} dt, \tag{A2}$$

where

$$x_{id} \equiv \frac{m_d v_s^2}{2T_d} = \frac{1}{2} \left(\frac{v_s}{v_d} \right)^2 = 1.77 \frac{m_d T_i}{m_i T_d}. \tag{A3}$$

From Eq. (A1), the magnitude of the total ion drag force on dust particles per unit volume is

$$F = \left(1 + \frac{m_i}{m_d} \right) \frac{4 \pi n_i n_d e^4 Z^2 \Gamma}{m_i v_s^2} \psi(x_{id}). \tag{A4}$$

The ion drag rate can be calculated from the relation $F \approx n_d m_d v_{di} v_s$ and Eq. (A4). We obtain

$$\nu_{\text{di}} = \left(1 + \frac{m_i}{m_d}\right) \frac{4\pi n_i e^4 Z^2 \Gamma}{m_d m_i v_s^3} \psi(x_{\text{id}}) \approx \frac{4\pi n_i e^4 Z^2 \Gamma}{m_d m_i v_s^3}. \quad (\text{A5})$$

From Ref. 13, we obtain the Coulomb logarithm

$$\Gamma \approx \frac{1}{2} \ln \left(\frac{\lambda_D^2 + b_{\pi/2}^2}{b_c^2 + b_{\pi/2}^2} \right), \quad (\text{A6})$$

where λ_D is the Debye length,

$$b_c \approx a_d \left(1 + \frac{2e(\phi_{\text{surface}} - \phi_{\text{plasma}})}{m_i v_s^2} \right)^{1/2} \quad (\text{A7})$$

is the collection impact parameter, and

$$b_{\pi/2} \approx e^2 Z / m_i v_s^2 \quad (\text{A8})$$

is the impact parameter corresponding to an asymptotic orbit angle of $\pi/2$. For the parameters given in Ref. 6, we have the inequality $b_c \ll b_{\pi/2} \approx 0.43 \mu\text{m} \ll \lambda_D \approx 15 \mu\text{m}$. Using this inequality and Eq. (A6), we obtain $\Gamma \approx 1.77$. When the Coulomb logarithm is this small, the accuracy of its calculation using Eq. (A6) is uncertain. However, lacking a better method of calculating the Coulomb logarithm, we will use this approach, with the understanding that the results may not be precise.

The total ion–dust collision force on ions is also given by Eq. (A4). We then obtain the collision rate,

$$\begin{aligned} \nu_{\text{id}} &= \left(1 + \frac{m_i}{m_d}\right) \frac{4\pi n_d e^4 Z^2 \Gamma}{m_i^2 v_s^3} \psi(x_{\text{id}}) \\ &\approx \frac{4\pi n_d e^4 Z^2 \Gamma}{m_i^2 v_s^3} = \frac{n_d m_d}{n_i m_i} \nu_{\text{di}} = \frac{\epsilon m_d}{m_i} \nu_{\text{di}}, \end{aligned} \quad (\text{A9})$$

which is the same as Eq. (5). For the experimental parameters given in Sec. IV, we obtain

$$\begin{aligned} \nu_{\text{id}} &\approx \frac{4\pi n_d e^4 Z^2 \Gamma}{m_i^2 v_s^3} \\ &= \frac{4\pi \times 10^7 \times (4.8 \times 10^{-10})^4 \times 75^2 \times 1.77}{(40 \times 1.67 \times 10^{-24})^2 \times (3.5 \times 10^4)^3} \\ &= 3.47 \times 10^5 / \text{s}. \end{aligned} \quad (\text{A10})$$

¹A. I. Akhiezer, I. A. Akhiezer, and V. V. Angeliko, *Sov. Phys. JETP* **30**, 476 (1970).

²J. C. Johnson, N. D'Angelo, and R. L. Merlino, *J. Phys. D* **23**, 682 (1990).

³G. Prabhuram and J. Goree, *Phys. Plasmas* **3**, 1212 (1996).

⁴P. K. Shukla and G. Morfill, *Phys. Lett. A* **216**, 153 (1996).

⁵N. D'Angelo, *Phys. Plasmas* **4**, 3422 (1997).

⁶D. Samsonov and J. Goree, *Phys. Rev. E* **59**, 1047 (1999).

⁷N. D'Angelo, *Phys. Plasmas* **5**, 3155 (1998).

⁸J. Goree, G. E. Morfill, V. N. Tsytovich, and S. V. Vladimirov, *Phys. Rev. E* **59**, 7055 (1999).

⁹A. V. Ivlev, D. Samsonov, J. Goree, G. Morfill, and V. E. Fortov, *Phys. Plasmas* **6**, 741 (1999).

¹⁰K. N. Ostrikov, S. V. Vladimirov, M. Y. Yu, and G. E. Morfill, *Phys. Rev. E* **61**, 4315 (2000).

¹¹A. V. Ivlev and G. Morfill, *Phys. Plasmas* **7**, 1094 (2000).

¹²K. Avinash, *Phys. Plasmas* **8**, 351 (2001).

¹³M. Barnes, J. H. Keller, J. C. Forster, J. A. O'Neil, and D. K. Coultas, *Phys. Rev. Lett.* **68**, 313 (1992).

¹⁴D. B. Graves and K. F. Jensen, *IEEE Trans. Plasma Sci.* **PS-14**, 78 (1986).

¹⁵This code is based on J. P. Boeuf and L. C. Pitchford, *Phys. Rev. E* **51**, 1376 (1995).

¹⁶P. Epstein, *Phys. Rev.* **23**, 710 (1924).

¹⁷M. J. Baines, I. P. Williams, and A. S. Asebiomo, *Mon. Not. R. Astron. Soc.* **130**, 63 (1965).

¹⁸See, for example, N. A. Krall and A. W. Trivelpiece, *Principles of Plasma Physics* (San Francisco Press, San Francisco, 1986), Chap. 6.